ELSEVIER

Nuclear Instruments and Methods in Physics Research A 355 (1995) 443–452

NUCLEAR INSTRUMENTS & METHODS IN PHYSICS RESEARCH Section A

After-pulse from helium-filled proportional counter at low temperatures near 4.2 K

Y. Isozumi [a,*], R. Katano [a], S. Ito [b], S. Kishimoto [c]

[a] *Institute for Chemical Research, Kyoto University, Uji, Kyoto 611, Japan*
[b] *Radioisotope Research Center, Kyoto University, Kyoto 606, Japan*
[c] *National Laboratory for High-Energy Physics, Photon Factory, Tukuba, Ibaraki 305, Japan*

Received 27 May 1994

Abstract

After-pulses, which appear in output signals from the helium-filled proportional counter (HFPC) cooled at low temperature (5–10 K), have been analyzed with a technique of non-linear least-squares fit; the drift time T_i of positive helium ions from anode to cathode, the spread in the drift time ΔT_i and the second Townsend ionization coefficient Γ_i of the positive ions have been determined. It is known that the carrier of positive charge in pure helium gas is the dimer ion He_2^+ at room temperature. We have found that T_i and ΔT_i are larger than the values estimated with the mobility of He_2^+ and Γ_i is much smaller than the value for He_2^+.

These results indicate that the carrier at low temperatures near 4.2 K is not He_2^+, but heavier molecular ions He_n^+; the size n is more than 10 in the present HFPC. It has been concluded that the cluster ion of large molecular helium plays an essential role in the proportional operation of HFPC, especially to suppress the continuous electric discharge. This self-suppression of discharge by the formation of cluster ions is discussed with some data of atomic and molecular heliums. The same quenching mechanism by cluster ions in other rare gases is also suggested.

1. Introduction

The helium-filled proportional counter (HFPC) is a useful tool to detect low-energy electrons at low temperatures (> 1.75 K), which has often been applied to cryogenic resonance-electron Mössbauer spectroscopy (REMS) [1,2]. According to the previous works [3–6], the operation of HFPC at low temperatures is summarized as follows:

i) Available gas gain is rather small; the maximum gain is at most 200 in the range of 2–23 K.

ii) The operation is limited by the continuous discharge, which takes place when the voltage applied to the anode is higher than a critical value (1270 V for the present HFPC). HFPC works stably as long as the anode voltage is below the critical value.

iii) The proportional operation transfers to the continuous discharge when the temperature of helium gas is higher than 23 K.

A counter filled with pure helium does not work in the proportional region at room temperature. To operate it with an available gas gain, some amount of admixture such as molecular organic gases is usually mixed in helium; the admixture is inevitable to achieve gas gains higher than 10^3 by quenching the continuous discharge, which is caused by secondary electrons emitted through the collision of ultra-violet photons, positive ions or metastables with cathode material. Our major concern is to understand why HFPC without any admixture works well at low temperatures. We have been trying to make clear the mechanism of the HFPC operation from the standpoint of atomic and molecular collision processes in pure helium.

In this paper, we report our recent study on the after-pulse from HFPC, indicating that the self-quenching mechanism of HFPC is attributed to the formation of positive helium cluster ions at low temperatures.

2. Observation

2.1. Apparatus

The present counter is the same one as used in the previous work [4], i.e., a cylindrical shape with an anode wire along its center line; the sensitive length is 60 mm, the diameter of the cathode is 25 mm and that of the anode

* Corresponding author. Tel. +81 774 32 311, fax +81 774 33 1247.

Elsevier Science B.V.
SSDI 0168-9002(94)01114-1

is 30 μm. The material of the cathode is stainless steel pipe and that of the anode is gold-coated tungsten wire. The filling gas is pure helium at normal condition, i.e., 760 Torr at room temperature (300 K); the gas density is 2.53×10^{19} 1/cm^3. To cool the filling gas near 4.2 K, the HFPC was mounted at the bottom of a liquid helium tank in a cryostat designed for REMS measurements. The temperature of helium gas in the HFPC was not measured precisely, but it was between 5–10 K. To pick up signals from the counter, a commercially available charge-sensitive preamplifier (Canberra 2003T) was used; the noise of the preamplifier is nominally 2.0 keV (FWHM, Si) with no capacitance. The whole noise contribution of the counter assembly including a 65 cm long signal cable (80 pF) is about 600 ion pairs.

5.3 MeV α rays from ^{210}Po were used to observe the after-pulses. A ^{210}Po source was installed at an end plate of the counter; the incident direction of the α particle is parallel to the anode after passing through a 1 mm diameter hole of collimator. The energy loss of the α rays in the present counter is about 1.5 MeV.

2.2. After-pulse

Pulse shapes of output signals from the preamplifier are shown by Fig. 1 (A), (B), (C) and (D), which were obtained with the anode voltage of 600 V, 800 V, 1000 V and 1200 V, respectively. The available maximum anode voltage for the present counter system is 1200 V; a few V over 1270 V always induces the continuous discharge. As seen in Fig. 1, there appears one bump on the shape (C) and three bumps on the shape (D). Those bumps are the after-pulses.

Each electron produced in the primary ionization of incident radiation is multiplied through the electron avalanche, which is caused by a steep electric field near the anode wire. Positive helium ions produced in the avalanche drift to the cathode, with which they collide emitting secondary electrons with a certain probability. Then, these secondary electrons drift to the anode wire where they cause new avalanches. Avalanches by the secondary electrons result in the first after-pulse in the shapes (C) and (D) of Fig. 1, while avalanches by the primary electrons result in the main pulse. Successive after-pulses are produced with the same mechanism as for the first after-pulse; the second and the third after-pulses are seen in the shape (D).

3. Analysis

3.1. Non-linear least-squares fit of pulse shape

In the non-linear least-squares fit [7] for analyzing output pulses from HFPC, the χ^2 function defined by

$$\chi^2 = \frac{1}{n-q} \sum_{j=1}^{n} w_j (M_j - V_j)^2 \qquad (1)$$

is minimized to deduce the most probable values of free parameters in theoretical model for the pulse shape, where M_j, $(j = 1, 2, \cdots, n)$ is the measured shape given by a set of pulse height at each time t_j, n is the total number of data and w_j is the weight for M_j. The theoretical model for the pulse shape is expressed by V_j $(a_1, a_2, \cdots, a_q)$ $(j = 1, 2, \cdots, n)$ in Eq. (1), where a_k $(k = 1, 2, \cdots, q)$ is the

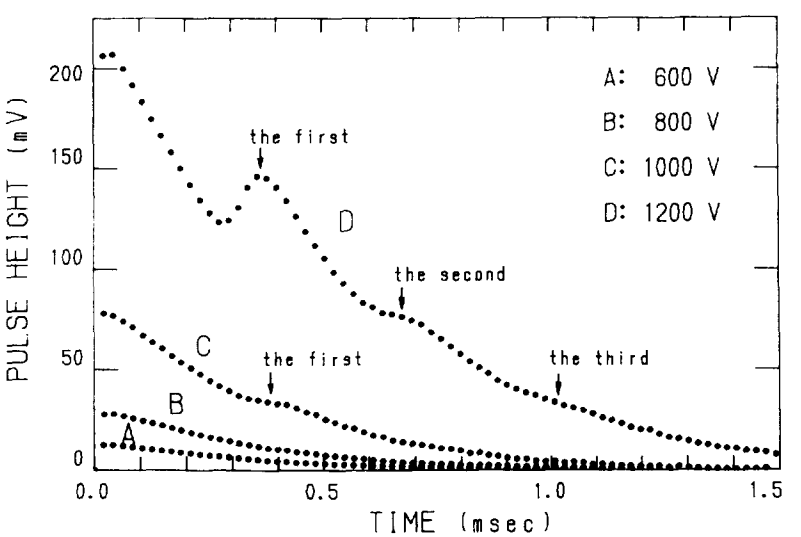

Fig. 1. Pulse shapes of output signals from the HFPC obtained with various anode voltages (600 V, 800 V, 1000 V and 1200 V). Bumps on the shapes (C) and (D) are after-pulses resulting from avalanches caused by secondary electrons, which are produced by the collision of positive helium ions with cathode material.

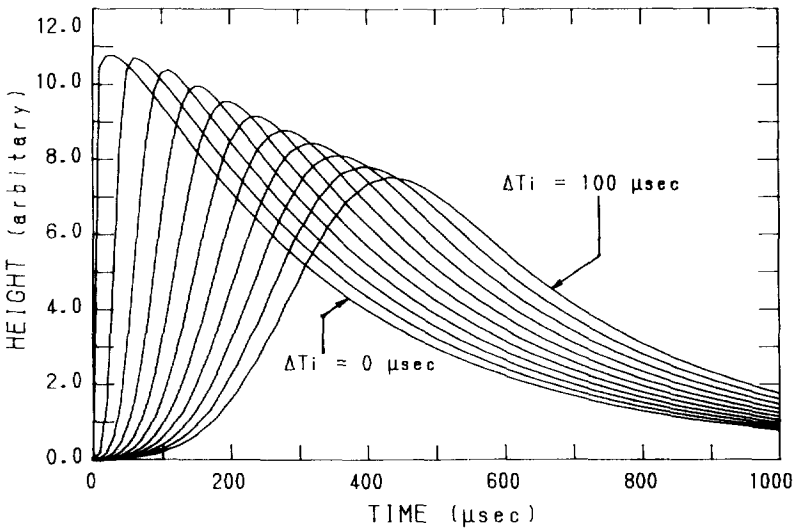

Fig. 2. Theoretical shape of the main and after-pulse as a function of the parameter ΔT_i (0–100 μs), which is defined as the spread in arrival time of positive helium ions at the cathode. The curve with $\Delta T_i = 0$ indicates the shape of main pulse given by Eq. (10) while those with $\Delta T_i \neq 0$ indicate the shape of the after-pulse given by Eq. (13) or (14).

free parameter in the model and q is the number of the parameters.

The error matrix for the most probable values is estimated from

$$(E)_{ij} = (L^{-1})_{ij}\chi^2, \quad (i, j = 1, 2, \cdots, q), \tag{2}$$

where $(L)_{ij}$ is the normal matrix deduced from the theory of statistics, i.e.,

$$(L)_{ij} = \sum_{k=1}^{n} w_k \frac{\partial V_k}{\partial a_i}\frac{\partial V_k}{\partial a_j}, \quad (i, j = 1, 2, \cdots, q). \tag{3}$$

3.2. Theoretical shape of output pulse

According to an approximate treatment of gas-filled counter [8], the output current from a cylindrical-shape proportional counter is given by

$$I(t) = \frac{Q}{(t + T_0)} \quad \text{for } 0 < t < T_i, \tag{4a}$$

$$= 0 \quad \text{for } T_i \leq t. \tag{4b}$$

In the above expression, Q is

$$Q = \frac{q}{2\ln(b/a)}, \tag{5}$$

where q is the total charge created by electron avalanches, a is the radius of anode wire and b is that of the cathode. The parameter T_0 is related to the period during which positive ions path through the steep electric field near anode wire:

$$T_0 = \frac{a^2 \ln(b/a)}{2\mu V_a}, \tag{6}$$

where μ is mobility of positive ion and V_a is voltage applied to anode. The parameter T_i is a mean time for the ions to drift from anode to cathode, which is equal to the time interval between the main and the first after-pulse or two successive after-pulses:

$$T_i = \frac{(b^2 - a^2)\ln(b/a)}{2\mu V_a}. \tag{7}$$

The voltage pulse from a charge-sensitive preamplifier is estimated as a convolution of the output current given by Eq. (4) and the impulse response of the preamplifier $w(t)$ [8]:

$$V_0(t) = \int_0^t w(t - \tau) I(\tau)\, d\tau. \tag{8}$$

In the above equation, $w(t)$ is approximately given by

$$w(t) = \frac{1}{C_f}\exp\left(-\frac{t}{T_f}\right), \tag{9}$$

where T_f [$\equiv R_f C_f$] is the decay constant of the preamplifier and R_f and C_f are feedback resistance and capaci-

Table 1
The most probable values and errors of parameters determined by the non-linear least-squares fit

Anode voltage	600 V	800 V	1000 V	1200 V
T_0 (ns)	0.20 ± 0.10	0.21 ± 0.10	0.17 ± 0.09	0.32 ± 0.19
T_f (μs)	288 ± 3	289 ± 3	285 ± 6	306 ± 6
A (mV) [a]	1.17 ± 0.05	2.62 ± 0.11	7.13 ± 0.28	19.8 ± 0.9
T_i (μs)	380 (fixed)	380 (fixed)	382 ± 2	323.8 ± 0.4
ΔT_i (μs)	–	–	26 ± 3	23 ± 2
R	–	–	0.088 ± 0.004	0.307 ± 0.008

[a] Amplitude of the pulse shape given by Eq. (15).

tance, respectively. Using Eq. (8), the shape of main pulse $V_0(t)$ is deduced as

$$V_0(t; T_0, T_f, T_i) = \frac{Q}{C_f}\exp\left(-\frac{t+T_0}{T_f}\right)\left(E_i\left(\frac{t+T_0}{T_f}\right) - E_i\left(\frac{T_0}{T_f}\right)\right) \quad \text{for } 0 < t < T_i, \tag{10a}$$

$$= \frac{Q}{C_f}\exp\left(-\frac{t+T_0}{T_f}\right)\left(E_i\left(\frac{T_i+T_0}{T_f}\right) - E_i\left(\frac{T_0}{T_f}\right)\right) \quad \text{for } T_i \le t, \tag{10b}$$

where $E_i(t)$ is the exponential integral defined by

$$E_i(t) = \int_{-\infty}^{t} \frac{1}{x}\exp(x)\,dx. \tag{11}$$

As seen in Fig. 1(D), the rise-time of the after-pulses is considerably longer than that of the main pulse. This comes from the fluctuation in the drift time T_i of positive helium ions. For the simplicity of calculation, this is neglected in the expression of the main pulse $V_0(t)$, i.e., Eq. (10). In the expression of after-pulses, the fluctuation is assumed to be given by a Gaussian:

$$G(\Delta T_i, t) = \frac{1}{\sqrt{2\pi}\,\Delta T_i}\exp\left\{-\frac{1}{2}\left(\frac{t}{\Delta T_i}\right)^2\right\}, \tag{12}$$

where $(\Delta T_i)^2$ is the covariance of the distribution and ΔT_i is a measure of the spread in the drift time T_i.

The shape of the first after-pulse is given by

$$V_1(t; T_0, T_f, T_i, \Delta T_i) = \int_{-\infty}^{+\infty} V_0(t; T_0, T_f, T_i + \tau)G(\Delta T_i, \tau)\,d\tau. \tag{13}$$

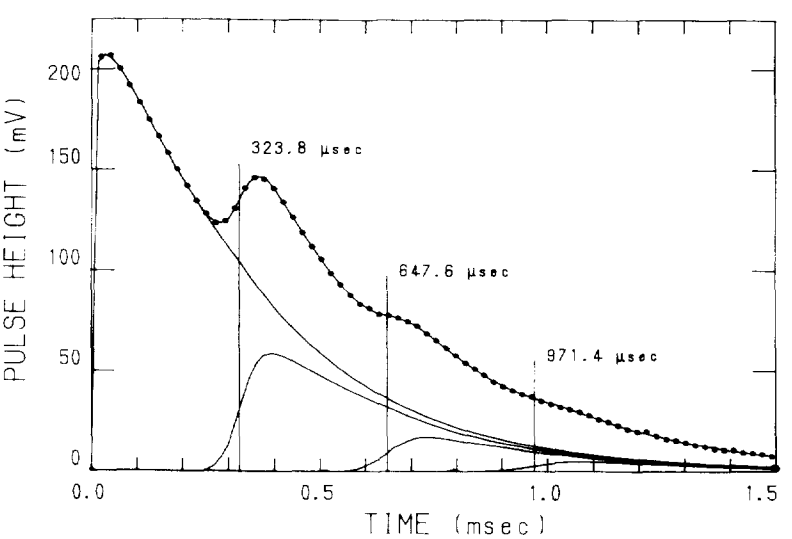

Fig. 3. Result of the non-linear least-squares fit for the composite pulse shape (D) obtained with V_a = 1200 V. The pulse is separated into four components: the main pulse, the first, the second and the third after-pulses.

Then, the nth after-pulse is

$$V_n(t; T_0, T_f, T_i, \Delta T_i) = \int_{-\infty}^{+\infty} V_0(t; T_0, T_f, nT_i + \tau) G\left(\sqrt{n}\,\Delta T_i, \tau\right) d\tau, \quad (14)$$

because the covariance of the nth after-pulse equals to $n(\Delta T_i)^2$ according to the Gauss distribution. Then, the composite shape of output pulse from the preamplifier is given by

$$V(t; T_0, T_f, T_i, \Delta T_i, R) = V_0(t; T_0, T_f, T_i) + \sum_{k=1}^{\infty} R^k V_k(t; T_0, T_f, T_i, \Delta T_i), \quad (15)$$

where R is the intensity ratio of the $(k-1)$th pulse to the kth pulse.

In Fig. 2 is shown the shape of the first after-pulse V_1 for various ΔT_i values ($\Delta T_i = 0$–100 μs). The rise time of V_1 is longer with increasing ΔT_i, as expected.

3.3. Reduced parameters

The measured pulse shapes (A), (B), (C) and (D) in Fig. 1 are resolved by the non-linear least-squares fit with the theoretical curve of Eq. (15); numerical results for most probable values of parameters and their probable errors are listed in Table 1. No after-pulse is separated from the shapes (A) and (B) while the first after-pulse is separated from the main pulse for the shape (C). In Fig. 3 is shown the result for the most complicated shape (D), which is well resolved into four components, i.e., the main pulse and the first, second, and third after-pulses.

The present data of pulse shapes are not sufficient to determine the parameter T_0, which is very sensitive to the rise-time part of pulse shape. This is a reason why the errors of T_0 in Table 1 are large. The T_f values deduced from shapes (A), (B) and (C) agree well with each other within probable errors. There is a distinct disagreement between the T_f value from the shape (D) and those from other shapes. The origin of this disagreement could not be revealed in the present work.

The parameters related to the after-pulse, i.e., T_i, ΔT_i and R, have been determined for anode voltages 1000 V and 1200 V with sufficient accuracy. These values are very useful to get information on the behavior of positive helium ions at low temperatures, as discussed below in detail.

4. Result and discussion

4.1. Drift time, T_i

Beaty and Patterson [9] measured the rate coefficient of the three-body reaction,

$$He^+ + He + He \rightarrow He_2^+ + He. \quad (16)$$

Their result of the coefficient is 1.08×10^{-31} cm^6/s at room temperature, from which the rate of the reaction in the present HFPC is estimated to 6.8×10^7 1/s. The life time of He^+ created by the electron avalanche in the present HFPC is at most 15 ns. This clearly indicates that, at room temperature, all He^+ ions in the avalanche are

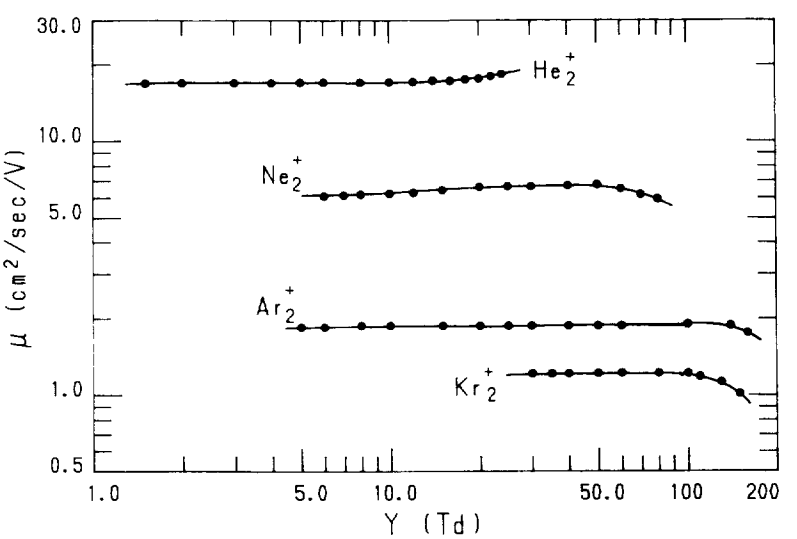

Fig. 4. Mobilities of dimer ions of rare gases in the same rare gases (He_2^+, Ne_2^+, Ar_2^+ and Kr_2^+), which are shown as a function of Y [$\equiv X/N_g$] (Td): X, field strength (V/cm); N_g, the gas density (1/cm^3); Td, 10^{-17} cm^2 s^{-1} V^{-1}.

transformed to the dimer He_2^+ in a very short time. In Fig. 4 are shown mobilities of dimer ions of rare gases in the same rare gases as a function of Y [$\equiv X/N_g$], where X is the field strength (V/cm), N_g is the gas density ($1/cm^3$): $\mu(He_2^+)$ [9], $\mu(Ne_2^+)$ [10], $\mu(Ar_2^+)$ [11], and $\mu(Kr_2^+)$ [12]. The quantity Y is usually given in the unit of Td [$\equiv 10^{-17}$ V cm^2].

The field strength X in a cylindrical counter is a function of the anode voltage V_a and radial distance from the symmetry axis r:

$$X(r) = \frac{V_a}{r \ln(b/a)}. \tag{17}$$

The drift velocity of positive ion is given by

$$\frac{dr}{dt} = \mu X(r), \tag{18}$$

where μ is the mobility of positive ions ($cm^2\ s^{-1}\ V^{-1}$). The drift time T_i is obtained by integrating dt of Eq. (18) from $r = a$ to $r = b$:

$$T_i = \frac{V_a}{N_g^2} \int_{Y(b)}^{Y(a)} \frac{dY}{\mu(Y) Y^3}. \tag{19}$$

For the present HFPC with $V_a = 1000$ V, Y is 390 Td at the anode ($r = a$) and 0.47 Td at the cathode ($r = b$). If the mobility μ is independent of Y, Eq. (19) equals to Eq. (7). As seen in Fig. 4, $\mu(He_2^+)$ is almost constant in the region of $Y \leqq 28.4$ Td and there is no data for higher Y. However, we can expect from $\mu(Ne_2^+)$, $\mu(Ar_2^+)$ and $\mu(Kr_2^+)$ in Fig. 4 that $\mu(He_2^+)$ for higher Y gradually decreases with increasing Y after passing a small bump near 30 Td. Eq. (19) indicates that $\mu(Y)$ in higher Y less contributes to the value of T_i, as long as $\mu(Y)$ does not decrease more steeply than the term Y^{-3} does. Then, approximating $\mu(He_2^+)$ to 16.7 $cm^2\ s^{-1}\ V^{-1}$, the drift time of He_2^+ in the HFPC is estimated as

$$T_i(He_2^+) = 315 \quad \mu s \text{ for } V_a = 1000 \text{ V}, \tag{20a}$$

$$= 263 \quad \mu s \text{ for } V_a = 1200 \text{ V}, \tag{20b}$$

where 16.7 $cm^2\ s^{-1}\ V^{-1}$ is an asymptotic value in the limit of $Y = 0$. Estimated T_i values are considerably smaller than the present results: 382 ± 2 μs for $V_a = 1000$ V and 323.8 ± 0.4 μs for $V_a = 1200$ V.

According to Eq. (7), T_i is inversely proportional to V_a when the mobility $\mu(Y)$ is a constant value. The experimental ratio of $T_i(1200\ V)/T_i(1000\ V) = 0.848 \pm 0.005$ agrees fairly well with 1000 V/1200 V = 0.833. Thus, we can except that the approximation mentioned above does not make a large error in estimating T_i.

4.2. Time spread, ΔT_i

In a simple treatment of drift and diffusion in the cylindrical counter, the distribution of positive ions in time and space is given by

$$F(r, t) = \frac{1}{4\pi Dt} \exp\left[-\frac{\{r - R(t)\}^2}{4Dt} \right], \tag{21}$$

where r is radial position in the counter, t is the period from the time when positive helium ions start to drift after electron avalanche, and D is the diffusion constant of the ions in helium gas. The function $R(t)$ is a mean position of the positive ions at the time t, which is deduced from

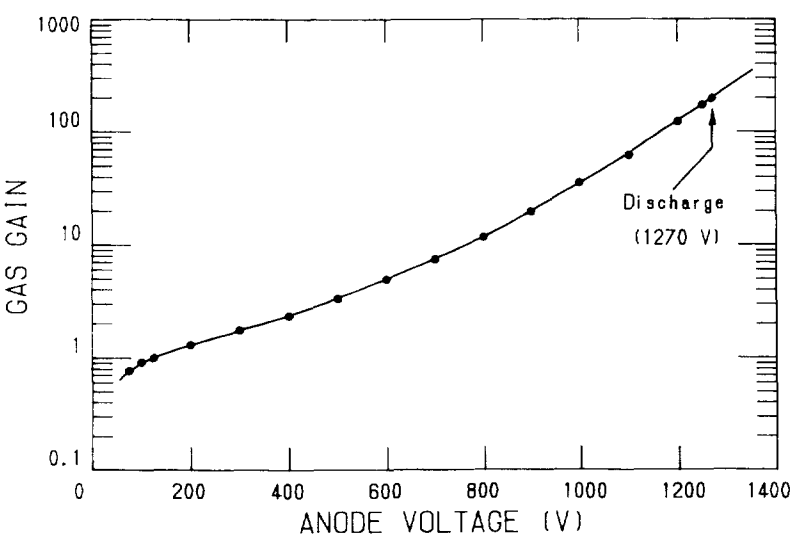

Fig. 5. The gas gain G as a function of anode voltage V_a measured with the present HFPC: temperature, 5–10 K; helium gas density, 2.53×10^{19} $1/cm^3$. The continuous discharge appeared at $V_a = 1270$ V.

the integration of Eq. (18), e.g., $b = R(T_i)$. An approximate distribution in time at the cathode ($r = b$) is deduced as

$$F(b, \Delta t) = \frac{1}{4\pi DT_i} \exp\left\{ -\frac{b^2(\Delta t)^2}{16DT_i^3} \right\}, \quad (22)$$

where $\Delta t \equiv t - T_i$. In the above derivation, we use the relations of $a \ll b$ and $\Delta t \ll T_i$. Comparing Eq. (22) with Eq. (12) and using the Einstein relation of

$$\frac{D}{\mu} = \frac{kT}{e}, \quad (23)$$

we obtain

$$\Delta T_i = [\ln(b/a)]^{3/2} \left(\frac{b^2}{\mu V_a} \right) \left(\frac{kT}{eV_a} \right)^{1/2}, \quad (24)$$

where k is the Boltzmann constant, T is the temperature of the gas and e is the electric charge.

Employing the same approximation as in the derivation of Eqs. (20a) and (20b), the parameter ΔT_i of He_2^+ in the HFPC at 5–10 K is estimated from Eq. (24):

$$\Delta T_i(He_2^+) = 1.1 \sim 1.5\ \mu s \quad \text{for } V_a = 1000\ V, \quad (25a)$$

$$= 0.7 \sim 0.9\ \mu s \quad \text{for } V_a = 1200\ V. \quad (25b)$$

These ΔT_i values are much smaller than the present results: 26 ± 3 μs for $V_a = 1000$ V and 23 ± 2 μs for $V_a = 1200$ V.

4.3. Coefficient Γ_i

The total charge produced by avalanches of the primary electrons is given by

$$q_1 = eGN_0, \quad (26)$$

where G is gas gain and N_0 is the number of electrons produced in the primary ionization by incident radiations. Since GN_0 equals to the number of positive ions drifting to cathode, the number of the secondary electrons is given by $GN_0\Gamma_i$, where Γ_i is the second Townsend ionization coefficient of the positive ion, i.e., a probability of the secondary electron emission through the collision of positive ions with the cathode. Then, the total charge produced by avalanches of the secondary electrons is expressed by

$$q_2 = eG^2N_0\Gamma_i. \quad (27)$$

The ratio of the height of the after-pulse to that of the main pulse equals to q_2/q_1:

$$R[\equiv q_2/q_1] = \Gamma_i G. \quad (28)$$

The gas gain G as a function of the anode voltage V_a has been measured with the same method as in the previous work [4]. Results are shown in Fig. 5. The ratio R determined by the present work is 0.088 ± 0.004 at $V_a = 1000$ V and 0.307 ± 0.008 at $V_a = 1200$ V while the gas gain G from Fig. 5 is 36 ± 2 at $V_a = 1000$ V and 123 ± 5 at $V_a = 1200$ V. With these values, we obtain the coefficient Γ_i of positive helium ion at low temperature (5–10 K):

$$\Gamma_i = (2.44 \pm 0.18) \times 10^{-3} \quad \text{at } V_a = 1000\ V, \quad (29a)$$

$$= (2.50 \pm 0.12) \times 10^{-3} \quad \text{at } V_a = 1200\ V. \quad (29b)$$

Hagstrum [13] measured coefficients Γ_i for the collision of helium ions with molybdenum. His result for He_2^+ is

$$\Gamma_i(He_2^+) = 0.13. \quad (30)$$

The cathode material of the present counter is stainless steel, which can be expected to have a Γ_i value of the same order as that for molybdenum. The present value is considerably smaller than the coefficient Γ_i of He_2^+, which is the carrier at room temperature. Thus, the secondary electron emission by the collision of positive helium ions with the cathode is greatly suppressed at low temperature.

4.4. Helium cluster ion

As shown in the above sections, there is a distinct difference between the present results for T_i, ΔT_i and Γ_i and the corresponding values for the dimer ions He_2^+. It is concluded that the carrier of positive charge in the HFPC cooled at the low temperature is not the dimer ion He_2^+. The rather large difference is attributed to the formation of positive molecular ions of helium at low temperatures, as discussed below.

When He^+ ions are injected in pure helium gas cooled at low temperatures, they are moderated in thermal energies by colliding repeatedly with helium atoms. Then, through successive reactions of

$$He_n^+ + He + He \rightarrow He_{n+1}^+ + He \quad (n = 1, 2, \cdots), \quad (31)$$

the molecular ion with larger size n grows up. In the equilibrium state, the number of the reaction (31) is balanced to that of its inverse i.e., decomposition of He_{n+1}^+. Therefore, the distribution of the number of He_n^+ as a function of the size n, i.e., size distribution, does not change in the equilibrium. Since the reaction (31) is exothermic, the equilibrium moves to larger n with lower gas temperature. The increase of gas density also moves the equilibrium to larger n because of the difference between the direct and inverse processes; the reaction (31) is a three-body reaction while its inverse is a two-body reaction. The size distribution depends on the field strength when the molecular ions drift in the electric field. The equilibrium moves to lower n in the higher electric field because of increasing kinetic energies of molecular ions.

With a quadruple mass spectrometer designed for low-temperature measurements, Kojima, Kobayashi and Kaneko

observed the size distribution of helium molecular ions ejected from the drift tube [14]. According to their data (Fig. 4 in Ref. [14]), the average of size n is about 10 at $T = 4.4$ K, $N_g = 1.36 \times 10^{17}$ 1/cm^3 and $Y = 1.14$ Td. The gas density in the present counter is 2.53×10^{19} 1/cm^3. which is the order of two larger than the value in the measurement by Kojima et al. Furthermore, Y at the cathode surface is 0.47 Td at $V_a = 1000$ V and 0.56 Td at $V_a = 1200$ V, i.e., about half of the value in their measurement. Thus, we can expect that the size of molecular ions colliding with the cathode in the present counter is larger than 10.

4.5. Mobility of cluster ion

The mobility of the positive ion mainly depends on the interaction potential between the positive ion and the neutral gas atom, which consists of the repulsive part of the short range and the attractive part of the long range [15].

The mobility in a limit neglecting the repulsive part is

$$\mu = \frac{39.5}{\sqrt{\alpha M_r}}. \tag{32}$$

where α is the polarizability of gas in a cubic of Bohr radius and M_r is the reduced mass measured in the unit of proton mass. The polarizability α comes from the polarization potential assumed for the long-range force

$$V(r) = -\frac{\alpha e^2}{2r^4}, \tag{33}$$

where r is the separation distance between the ion and the gas atom. Eq. (32) holds in the double limit of low temperature and low Y [$\equiv X/N_g$]. Inserting 2.05×10^{-24} cm^3 for α and 4 for M_r into Eq. (31), the mobility is estimated to 15.3 cm^2 s^{-1} V^{-1}. With this mobility, we obtain $T_i = 343$ μs for $V_a = 1000$ V and $T_i = 286$ μs for $V_a = 1200$ V from Eq. (7), which are still smaller than the present results in Table 1.

In a limit neglecting the attractive part, the mobility is approximately given by

$$\mu = 0.75\left(\frac{e\lambda_i}{v}\right)\frac{1}{\sqrt{M_r M_i}}, \tag{34}$$

where λ_i and M_i are the mean free path and mass of the positive ion, respectively, v is average thermal velocity and M_r is reduced mass of ion and gas atom. According to Eq. (34), the mobility is proportional to $\lambda_i M_i^{-1/2}$ in a limit of large M_i; note that $v = (8kT/\pi M_g)^{1/2}$ and $M_r = M_i M_g/(M_i + M_g)$, where T is temperature of the ion and M_g is the mass of the gas atom. The mean free path λ_i is defined by $1/(\Omega N_g)$, where Ω is the cross section of elastic collision between ion and gas atom and N_g is the gas density. In the rigid sphere model, Ω is the geometrical cross section of cluster ions, which is roughly proportional to $M_i^{2/3}$. Thus, the mobility μ decreases as $M_i^{-7/6}$ and the drift time T_i increases as $M_i^{7/6}$ when M_i becomes very large. It is clear that the T_i values obtained by the present work are enhanced by the formation of cluster ions. It is interesting to estimate the mobility of helium ion clusters from more refined theoretical treatments such as Chapman–Enskog theory [15], in which the whole shape of the interaction potential can be taken into account.

The influence of the growth of clusters on the mobility of positive ions at higher temperatures was already examined by Hutton [16].

4.6. Mechanism of electron ejection from cathode

Electron ejection by collision of slow atomic ions with metal was investigated both experimentally and theoretically by many workers [17]. Two mechanisms were proposed for ions of rare gas atoms: (i) Auger neutralization of ionized atom and (ii) resonance neutralization of the atom followed by Auger de-excitation. The first is the one-step process in which an electron in the conduction band of metal is directly transferred to the ground state of the atom, another electron in the band emitting to the

Table 2
Separation energy of an atom from molecular ion of rare gas atom

$n \rightarrow (n-1)$	Separation energy (meV)				
	He	Ne	Ar	Kr	Xe
2 → 1	2360 [1]	1360 [1]	1270 [1]	1150 [1]	1030 [1]
3 → 2	162 ± 7 [2]	107 ± 7 [2]	212 ± 7 [3]	241 ± 7 [2]	261 ± 7 [2]
4 → 3	28 ± 7 [2]	34 ± 7 [2]	72 ± 7 [3]	94 ± 7 [2]	114 ± 7 [3]
5 → 4	21 ± 7 [2]	33 ± 7 [2]	70 ± 7 [3]	89 ± 7 [2]	–
6 → 5	–	33 ± 7 [2]	70 ± 7 [3]	88 ± 7 [2]	–
7 → 6	–	33 ± 7 [2]	69 ± 7 [3]	–	–
8 → 7	–	31 ± 7 [2]	69 ± 7 [3]	–	–
9 → 8	–	29 ± 7 [2]	68 ± 7 [3]	–	–
10 → 9	–	27 ± 7 [2]	67 ± 7 [3]	–	–
11 → 10	–	–	67 ± 7 [3]	–	–

continuum. The second is the two-step process, in which an electron in the band is transferred resonantly to the excited state of the atom by the tunnel effect and then the atom de-excites to the ground state emitting another electron in the band to the continuum. The transition probability of the first process is usually much larger than that of the second process. No works were performed on the collision of large molecular ions of rare gas atoms with metal. However, it can be expected that, in the collision of the cluster ions, the energy released in the process is mostly consumed by decomposing the cluster rather than emitting an electron into the continuum. Thus, the small coefficient Γ_i given by Eqs. (29a) and (29b) is caused by a much larger channel of decomposing the cluster ions rather than the Auger neutralization; the coefficient Γ_i is probably smaller as the size of cluster n is larger.

4.7. Cluster ions of other rare gases

In Table 2 are listed separation energies of rare gas cluster ions Rg_n^+ [Rg = He, Ne, Ar, Kr or Xe] [18–20], which is defined as an energy to separate an atom from the cluster ion as a function of the size n. The separation energy decreases as n increases. Note that the changes in energy between $n = 2 \rightarrow 1$ and $n = 3 \rightarrow 2$ are very large and then the energy becomes almost constant for $n > 3$, as seen in the cases of Ne, Ar and Kr. This behavior indicates that the chemical bond for an atom in the ions of Rg_2^+ and Rg_3^+ is covalent rather than electrostatic and then becomes pure electrostatic for the cluster ions with $n > 3$. The separation energy at $n = 4$ is 28 meV for He, 34 meV for Ne, 72 meV for Ar, 94 meV for Kr and 114 meV for Xe, increasing rather steeply for heavier rare gas elements.

In the previous works, it was found that the counter filled with pure helium works in the temperature region of 2–23 K [3–6] and that with pure neon works in the region of 20–45 K [21]. The temperature region depends on the cluster size; as the separation energy is higher, larger cluster ions can exist at higher temperatures. No study has so far been reported on the temperature region for Ar, Kr and Xe. However, the behavior of the separation energy shown in Table 2 suggests that these gases with no admixture may operate the counter even at room temperature. In fact, some workers who extensively use gas-filled counters know that a counter filled with pure Ar, Kr or Xe operates well with low gas gains at room temperature. Experiments to observe the after-pulses from the counter filled with these rare gases will make clear if the self-quenching at room temperature is caused by the formation of large cluster ions or not.

5. Concluding remarks

To understand the operation of HFPC more in detail, it is necessary to reveal the mechanism of the continuous discharge caused by applying a high voltage to the anode. According to the theory of electric discharge, the source of the discharge is ion, photon or metastable; any avalanche grows up to the electric discharge when the number of secondary electrons from cathode per avalanche, i.e., R defined as Eq. (28), is more than unity. The role of metastables may be neglected in a gas with a so high density as in the present counter (2.53×10^{19} $1/cm^3$) because most of them are de-excited by the collision with normal helium atoms. The present work has clearly shown that the helium ion is not the source of the discharge at low temperatures (5–10 K); the present result for R [$\equiv \Gamma_i G$] is 0.308 at $V_a = 1200$ V, which is near the critical voltage (1270 V) to induce the discharge. We have very recently performed detailed analyses of the continuous discharge, revealing that the discharge is caused by photons which mainly consist of non-resonant radiations from highly-excited helium atoms produced in electron avalanches. Results of the analyses will be given elsewhere.

Thus, the operation of HFPC is limited by the number of secondary electrons emitted by collisions of the positive ion and the photon with the cathode. The temperature limit of the HFPC operation, i.e., 23 K, means that R is larger than unity at this temperature. In the present situation, it is not clear which is the source of the discharge at 23 K, positive ions or photons. The refined measurement of Γ_i by the present method and the observation of the discharge pulse in the temperature region from 4.2 K to 25 K are now in plan.

References

[1] The proportional counter technique for REMS is reviewed in G.N. Belozerski, Mössbauer Studies of Surface Layers (Elsevier, Amsterdam, 1993) p. 220.
[2] Typical applications of HFPC to REMS are seen in T. Kobayashi, K. Fukumura, Y. Isozumi and R. Katano, Hyperfine Interactions 57 (1990) 1923;
T. Fujii, M. Takano, R. Katano, Y. Bando and Y. Isozumi, J. Appl. Phys. 68 (1990) 1735.
[3] Y. Isozumi, S. Kishimoto, R. Katano and H. Takekoshi, Rev. Sci. Instr. 58 (1987) 293.
[4] S. Kishimoto, Y. Isozumi, R. Katano and H. Takekoshi, Nucl. Instr. and Meth. A 262 (1987) 413.
[5] Y. Isozumi, S. Ito, T. Fujii and R. Katano, Rev. Sci. Instr. 60 (1989) 3262.
[6] K. Fukumura, R. Katano, T. Kobayashi, A. Nakanishi and Y. Isozumi, Nucl. Instr. and Meth. A 301 (1991) 482.
[7] Theoretical discussion on the non-linear least-squares fit for spectrum analysis is reviewed in Y. Isozumi, Nucl. Instr. and Meth. A 235 (1985) 164.
[8] E. Kowalski, Nuclear Electronics (Springer, Berlin, 1970).
[9] E.C. Beaty and P.L. Patterson, Phys. Rev. A 137 (1965) 346.
[10] E.C. Beaty and P.L. Patterson, Phys. Rev. 170 (1968) 116.
[11] E.C. Beaty, Proc. 5th Int. Conf. on Ionization Phenomena

Gases, Munich, 1961, Vol. 1 (North-Holland, Amsterdam) p. 183.
[12] M.A. Biondi and L.M. Chain, Phys. Rev. 94 (1954) 910.
[13] H.G. Hagstrum, Phys. Rev. 89 (1953) 244.
[14] N. Kobayashi, T. Kojima and Y. Kaneko, J. Phys. Soc. Japan 57 (1988) 1528.
[15] Various theories on the mobility of positive ions are viewed in E.W. McDaniel, J.B. Michell and M.E. Rudd, Atomic Collision (Heavy Particle Projectiles) (Wiley, New York, 1993) p. 485.
[16] P.G. Hutton, Proc. Phys. Soc. London 82 (1963) 526.
[17] H.D. Hagstrum, Phys. Rev. 96 (1954) 336.
[18] R.G. Keesee and A.W. Castleman, Jr., J. Phys. Chem. Ref. Data 15 (1986) 1011.
[19] K. Hiraoka and T. Mori, J. Chem. Phys. 92 (1980) 4408.
[20] K. Hiraoka and T. Mori, J. Chem. Phys. 90 (1989) 7143.
[21] K. Fukumura, A. Nakanishi, T. Kobayashi, R. Katano and Y. Isozumi, Nucl. Instr. and Meth. B 61 (1991) 127.